Materials Research Express

Fabrication of an acetone gas sensor based on Si-doped WO_3 nanorods prepared by reactive magnetron co-sputtering with OAD technique

Materials Research Express

PAPER

Fabrication of an acetone gas sensor based on Si-doped WO_3 nanorods prepared by reactive magnetron co-sputtering with OAD technique

Waraporn Sucharitakul[1], **Anupong Sukee**[1], **Pimchanok Leuasoongnoen**[2], **Mati Horprathum**[3], **Tossaporn Lertvanithphol**[3], **Pattanaphong Janphuang**[2], **Pusit Mitsomwang**[4] and **Bura Sindhupakorn**[5]

[1] School of Biomedical Engineering Innovation, Suranaree University of Technology, 111 University Avenue, Muang District, Nakhon Ratchasima, 30000, Thailand
[2] Synchrotron Light Research Institute, 111 University Avenue, Muang District, Nakhon Ratchasima, 30000, Thailand
[3] National Electronics and Computer Technology Center (NECTEC), Phahonyothin Road, Khlong Nueng, Khlong Luang, Pathumthani, 12120, Thailand
[4] School of Metallurgical Engineering, Suranaree University of Technology, 111 University Avenue, Muang District, Nakhon Ratchasima, 30000, Thailand
[5] Center of Excellence in biomechanics medicine, School of medicine, Suranaree medical institute, 111 University Avenue, Muang District, Nakhon Ratchasima, 30000, Thailand

E-mail: bura@sut.ac.th

Keywords: Si-doped WO_3 nanorods, oblique-angle deposition (OAD), acetone gas sensor

OPEN ACCESS

RECEIVED
5 November 2021

REVISED
15 December 2021

ACCEPTED FOR PUBLICATION
20 December 2021

PUBLISHED
31 December 2021

Abstract

Gas sensing technology is currently applied in a variety of applications. In medical applications, gas sensors can be used for the detection of the biomarker in various diseases, metabolic disorders, diabetes mellitus, asthma, renal, liver diseases, and lung cancer. In this study, we present acetone sensing characteristics of Si-doped WO_3 nanorods prepared by a DC reactive magnetron co-sputtering with an oblique-angle deposition (OAD) technique. The composition of Si-doped in WO_3 has been studied by varying the electrical input power applied to the Si sputtered target. The nanorods film was constructed at the glancing angle of 85°. After deposition, the films were annealed at 400 °C for 4 h in the air. The microstructures and phases of the materials were characterized by x-ray photoelectron spectroscopy (XPS), x-ray diffraction (XRD), and field-emission scanning electron microscopy (FESEM). The results showed that 1.43 wt% Si-doped WO_3 thin film exhibited the maximum response of 5.92 towards 100 ppm of acetone at performing temperature (350 °C), purifying dry air carrier. The process exposed in this work demonstrated the potential of high sensitivity acetone gas sensor at low concentration and may be used as an effective tool for diabetes non-invasive monitoring.

1. Introduction

At present, the burden of diabetes has been rapidly increasing. The global prevalence of diabetes has been rising from 4.7% in 1980 to 8.5% in 2014. Over 420 million world populations are facing diabetes. Forecasting in 2030, demonstrates that more than 570 million people have been living with diabetes [1]. Diabetes is a chronic disease, caused by a deficiency of insulin secretion and insulin resistance. Diabetes patients who poorly control blood glucose lead to increased risks of other diseases including heart, retinopathy, nephropathy, and neuropathy and nerve, increasing limb amputation. The current standard diabetes diagnostic method is to analyze the amount of insulin by pricking blood at the fingertips. This method is an invasive technique, very painful, expensive, and may be infected. A non-invasive method by human breath analysis became more interesting for detecting various volatile organic compounds that were a biomarker for detecting different diseases such as metabolic disorders, diabetes mellitus, asthma, renal and liver diseases, and lung cancer. Human exhaled breath contains

Table 1. Sensing performances of WO_3 and Si-doped WO_3 towards acetone detection.

Materials	Conc. (ppm)	Temp. (°C)	Response	References
WO_3 microsphere	150	200	56%	[18]
WO_3 nanostructure	100	200	7	[19]
Single WO_3 crystal	1000	307	20	[20]
WO_3 nanoplate	1000	300	42	[21]
Si-doped εWO_3	0.6	400	4.63	[16]
Si-doped WO_3	8	425	40.53	[17]
Si-doped WO_3 (this work)	100	350	5.92	

nitrogen, oxygen, carbon dioxide, ammonia, hydrogen sulfide and other volatile organic compounds such as acetone [2, 3].

We monitored blood sugar levels in Diabetes mellitus (DM). The blood-sugar level is related to the ketone bodies which consist of acetoacetate, beta-hydroxybutyrate, and acetone [4]. Acetone level in the breath for healthy people is in the range of 0.5–0.9 ppm and above 1.25–2.5 ppm for diabetes patients [5]. The medical reports showed that 40 ppm of acetone was found in normal people who eat ketogenic diet (high cholesterol), 360 ppm in children with seizures, and 1250 ppm in poorly controlled diabetic patients with ketoacidosis. Thus, the concentration of breath acetone below 0.9 ppm can be screening diabetes. There were several methods to measure breath acetone levels. The various techniques used to analyze acetone in the breath to diagnose diabetes such as Gas chromatography with mass spectrometry (GC-MS), Selected ion flow tube mass spectrometry (SIFT-MS), Proton transfer reaction with mass spectrometry (PTR-MS), Light-addressable potentiometric sensors (LPAS), and Semiconductor metal oxide sensor (SMOS) measured in part per million (ppm), part per billion (ppb), and part per trillion (ppt) [6].

In recent years, metal oxide semiconductor-based gas sensor is of great interest and widely used in portable acetone detection. Their advantages were a smaller size, higher sensitivity, lower cost, better reversibility, and easier operation compared to the other techniques, such as gas chromatography and mass spectrometry [7]. Therefore, many researchers have focused on the application of semiconductor metal oxide-based gas sensors in patients with diabetes. There are several metal oxides considered as a sensing material for monitoring acetone gas, including WO_3, CuO, SnO_2, and TiO_2 [8–11]. Their performances have been improved in terms of sensitivity and selectivity by additives or applied appropriate working temperature for target gas. Many studies have focused the sensing improvements via surface and microstructure modifications by doping and loading.

Tungsten oxide (WO_3) is one of the promising candidate metal oxides to be used as a sensing layer because of its physical and chemical properties, especially in acetone gas sensing applications. Haiyun Xu *et al* [12] have reported acetone gas sensors based on mesoporous WO_3 nanofiber with the crystalline framework and aqueous phase by an electrospinning process. The result showed a fast response time (24 s) and recovery time (27 s) to a relatively low acetone concentration of 1 ppm at 300 °C. Similarly, Chang X *et al* [13] created WO_3 nanosheets of inorganic fullerene-like WS_2 particle prepared by sulfurization of WO_3 nanoparticle that showed the fast response time (6 s) and recovery time (9 s) to a slightly low level of acetone concentration (0.17 ppm at 300 °C.11 M). Imran *et al* [14] used acetone sensor-based non-stoichiometric tungsten oxide (WO_3-x) nanofibers prepared by electrospinning. It showed that the sensor had repeatability of more than 99% towards low acetone concentration at 350 °C. Moreover, J Shi *et al* [15] have developed WO_3 nanocrystals by the sol-gel method for acetone detection. The sensor exhibited a super low acetone detection limit at 0.05 ppm at 300 °C.

There was a report demonstrating that WO_3 surface modification by Si additive resulted in improvement of acetone response as shown in table 1. M Righettoni *et al* [16] have reported acetone gas sensor based on Si-doped εWO_3 phase prepared by flame spray pyrolysis. The sensor response is 4.63 at 600 ppb in dry air and 0.7 in 90% RH at the temperature of 400 °C. In addition, A Rydosz *et al* [17] have reported acetone gas sensors based on Si-doped WO_3 prepared by glancing angle DC magnetron sputtering method. The sensor showed the maximum response of 40.53 towards 8 ppm acetone at 425 °C.

In this work, we prepared Si-doped WO_3 nanorods by magnetron sputtering as a sensitive layer for acetone detection. The magnetron sputtering presented advantages with a homogeneous morphology, easily controlled the thickness of the films, and could be manipulated the composition of each deposited material by controlling the applied power to the sputtering sources [22, 23]. The acetone gas sensing performance has been characterized to demonstrate the potential of Si-doped WO_3 nanorods as a high sensitivity acetone gas sensor at low concentration and can be used as a non-invasive method for diabetes monitoring.

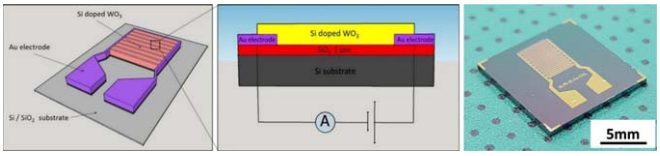

(a) (b)

Figure 1. (a) Schematic diagram of sensor design in this work (b) an optical image of fabricated sensor.

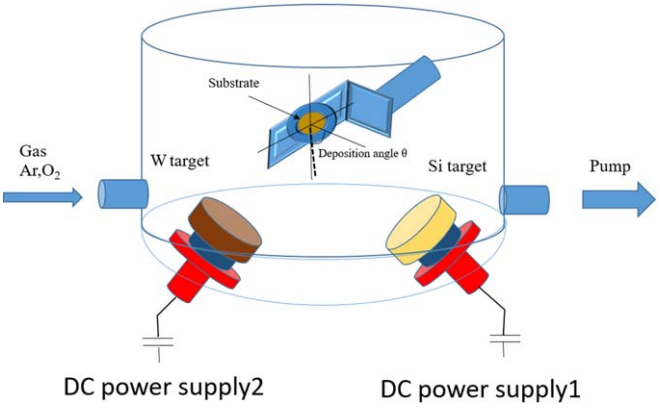

Figure 2. Schematic diagram of reactive magnetron co-sputtering with OAD deposition technique.

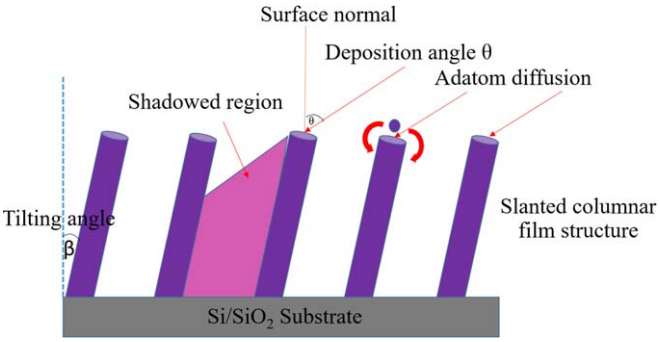

Figure 3. Shadowing effect and surface diffusion and Si-doped WO_3.

2. Experimental

2.1. Design and fabrication of an acetone gas sensor based on Si-doped WO3 nanorods

The design of the sensor was shown in figure 1(a). It consisted of a sensitive element and pairs of gold (Au) interdigitated electrodes, with interspacing between fingers of 100 μm and had an active area with approximately 3250 μm $\times$ 4000 μm, fabricated on a silicon wafer with a SiO_2 buffer layer. The fabrication process, after standard cleaning of Si wafer, 1 μm- thick SiO_2 insulating layer was grown by thermal oxidation protecting the electrical connection between the substrate (Si) and the electrode. The interdigitated electrodes were patterned by photolithography and followed by lift-off of deposited 150 nm-thick Au by electron beam evaporation. Then, a sensitive layer made of WO_3 was deposited on top of Au interdigitated electrodes using reactive magnetron co-sputtering with oblique angle deposition (OAD) technique as described in figure 2. It was used for single-step film deposition via oblique angle physical vapor deposition with precision substrate rotation. This process provides nanorod fabrication with good dispersion [24].

During the film deposition process, the nanorods could be formed on the surface at oblique angles. Due to the shadowing effect, the particles were captured at higher surface points [25, 26], leading to form rougher surfaces with columnar structures as shown in figure 3. In the reactive magnetron co-sputtering with OAD

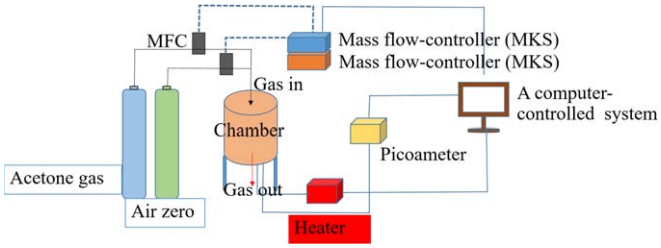

Figure 4. The measurement system of sensors characteristics and gas installation.

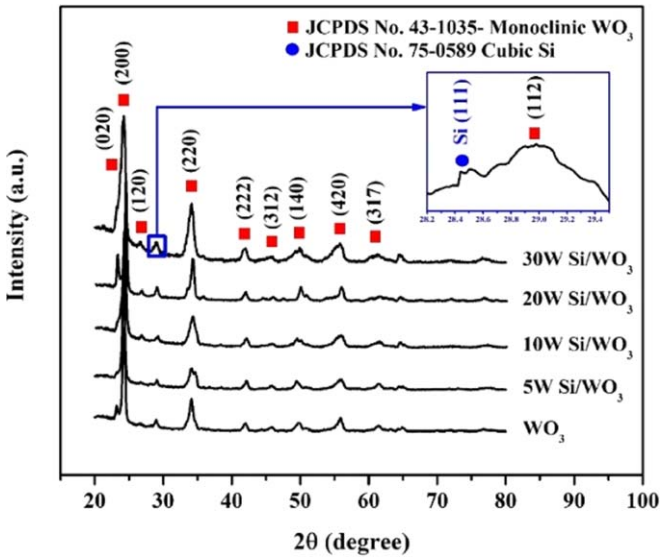

Figure 5. XRD patterns of the as-deposited Si-doped WO_3 nanorods with varying the input power from 5 W to 30 W) to Si target.

procedure, nanorods were fabricated at oblique angle deposition producing arrays of nanorods with rough surfaces. The fabricated sensor used in this work was shown in figure 1(b).

The Si-doped WO_3 nanorods have been deposited by reactive magnetron co-sputtering (AJA international, Inc.; ATC 2000-F) with the OAD configuration. In the sputtering deposition process, the vacuum chamber was initially evacuated to a base pressure of 6.0 × 10–6 Tor. Sputtered targets made of 2-inch-diameter and 0.250-inch-thick Tungsten (99.99% purity), and 2 inch-diameter and 0.250-inch-thick Silicon (99.99% purity) was used as sputtered targets. Both sputtered targets aligned to the center of the substrate surface in OAD geometry with a deposition angle of 85°. The W target was set at a distance of 69 mm from the centreline of the substrate. A sputtering pulse DC power of 150 W was initially applied to the tungsten target while varying input DC power from 0–30 W to silicon target. The chamber was filled with Argon (Ar) and oxygen (O_2) to ignite the plasma and act as a reactive gas. The Si-doped WO3 films were deposited with a constant ratio of 68% Ar/32% O2. The flows of Ar and O_2 were precisely controlled by mass flow controllers. The deposition pressure was maintained at 5×10^{-3} Tor and the duration of deposition pressure was set at 72 min to achieve 500 nm film thickness. The sample was deposited at room temperature. Subsequently, the as-prepared samples were annealed at 400 °C in the air for 4 h.

The physical properties of the films were characterized by using an x-ray diffractometer (XRD) to point out the amorphous and crystalline states of the films.

A field-emission scanning electron microscope (FESEM) was used to examine their superficial morphologies and nanostructures. The film's composition was analyzed by using Energy Dispersive x-ray Spectroscopy (EDS). The oxidation state of element composition was characterized by x-ray Photoelectron Spectroscopy (XPS). The binding energy was calibrated with C 1 s reference (284.8 eV).

2.2. Gas-sensing measurement

The acetone gas sensing performance of Si-doped WO_3 nanorods was studied by using a gas sensing measurement system presented in figure 4. Briefly, the target acetone concentration was achieved by mixing clean dry air (Air zero) with an acetone gas balanced in dry air at a T-junction connector using multichannel

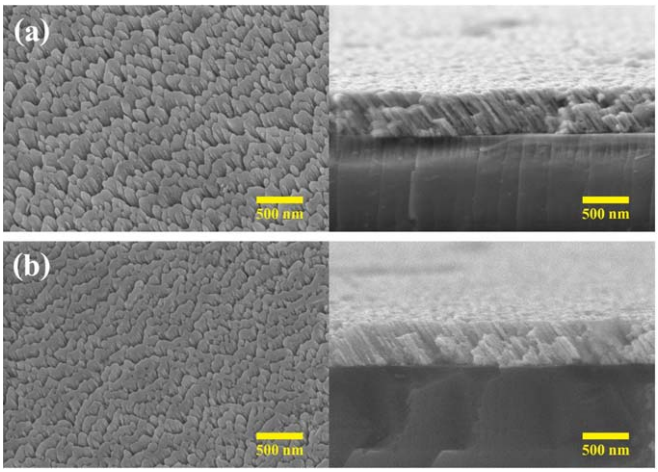

Figure 6. FE-SEM surface morphology and cross-section images of (a) pure WO_3 and (b) Si-doped WO_3 nanorods deposited onto the sensor substrate after annealing.

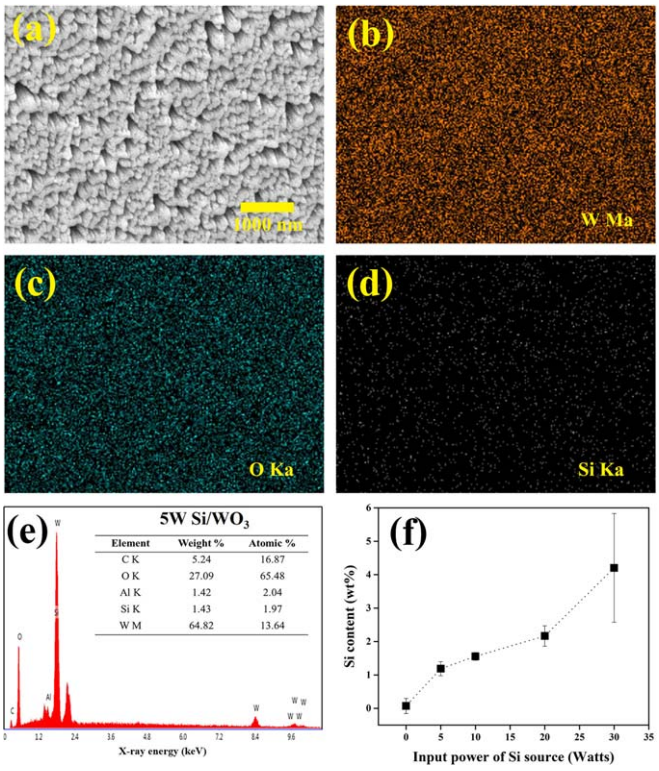

Figure 7. (a) Surface morphology and EDS map showing element contribution of (b) W Ma, (c) O Ka, and (d) Si Ka and (e) EDS spectra of the 5 W Si/WO_3 sample. (f) Si content (wt%) versus Input power of Si source.

mass flow controllers. The targeted concentration has flowed to the test chamber (2000 sccm) with a flow rate of 2 l/min). The electrical resistance of the sensor was monitored using a digital electrometer. The sampling time was set to 1 s. The resistance was measured at an operating temperature ranging from 250 °C to 400 °C as a function of acetone concentration in a range from 50 ppm to 100 ppm. The sensor response(S) to acetone was determined as the resistance ratio $S = Rair/Rgas$, where Rair was the resistance of the sensor in the air zero and Rgas was the resistance of the sensor upon exposure to the acetone gas. The response time is given by a time that attains 90% of the stabilized signal after gas exposure while the recovery time is defined by a time that attains 90% of the stabilized signal after air recovery.

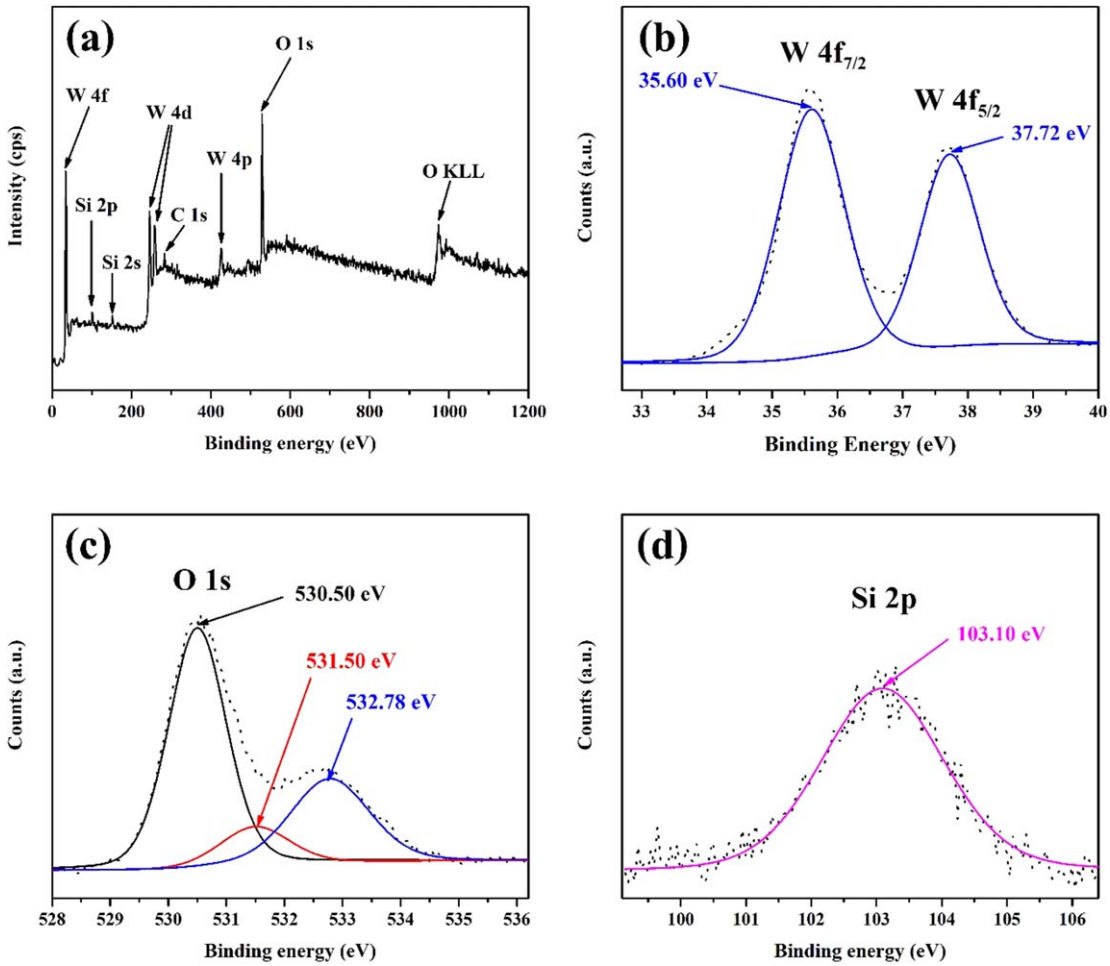

Figure 8. (a) XPS survey scan spectrum and high-energy resolution core-level spectra: (b) W 4 f, (c) O 1 s and (d) Si 2p of 5 W Si/WO_3 sample.

3. Results and discussion

3.1. Structure and micro- morphology characterization

The XRD patterns of Si-doped WO_3 at different Si weight% compositions by varying the input power to Si target (5–30 W) are shown in figure 5. It was obvious that strong and sharp diffraction peaks were observed indicating the sample was highly crystalline. The XRD patterns of the prepared samples could be matched to a monoclinic phase of WO_3 (JCPDS no. 43–1035), displaying the dominant planes of (020), (200), (120) (220), (312), (140), (420) and (317) as shown in figure 5. Furthermore, the XRD pattern of Si-doped WO_3 nanorods confirms that Si was presented in metallic Si (Si°) state, which was indexed to the face centered cubic structure of Si (JCPDS no.75–0589), with the plane of (111). The appearance of the Si diffraction peaks indicates that the silicon particles may be supported on the surface of tungsten trioxide.

In order to verify surface morphologies and nanostructures, the composition and particularly the doping content of an obtained sample, FE-SEM and EDS were carried out as shown in figures 6–7. Figure 6. shows the typical morphology and cross-section of pure and Si-doped WO_3 films. The SEM image of pure WO_3 (figure 6(a)) shows that the surface contains lots of nanorods homogenously distributed on the substrate. For Si-doped WO_3 (figure 6(b)), some nanorods were connected. The film thickness was found to be approximately 500 nm and nanorods were deposited on the substrate with an angle of 42 degrees

Figures 7(a)–(e) illustrated the EDS maps and EDS spectra taken from the top-view surface morphology of Si-doped WO_3 (5 W Si/WO_3 sample) after deposition and annealing at 400 °C in air. The corresponding EDS maps of W and O elements indicated homogeneous distributions of the components over the scanned region, while the distribution of Si element is visible with low intensity. The EDS spectra indicate the characteristic x-ray peaks corresponding to O, W, and Si atoms present in the sample and a small peak from C, which is derived from carbon tape used to hold the sample during the measurement. From the EDS analysis, the amount of Si was found to be 1.43 weight% (1.97 atomic%) for sample deposited input power 5 watts of Silicon target which is in

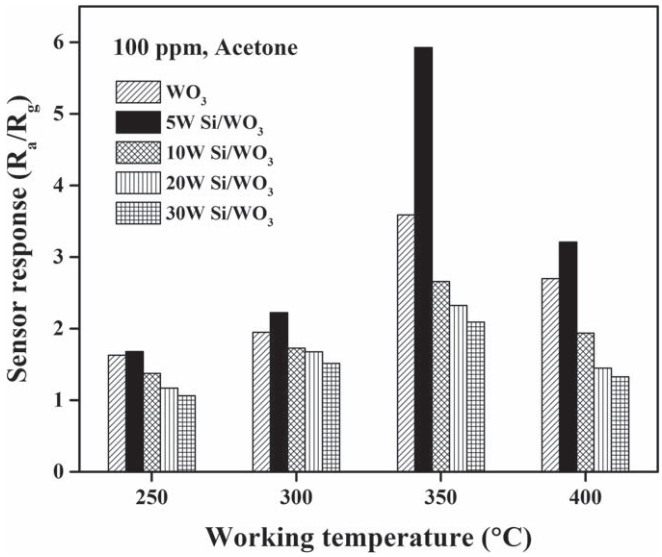

Figure 9. The response of the optimal Si-doped WO_3 nanorods in the acetone concentration of 100 ppm at different operating temperatures.

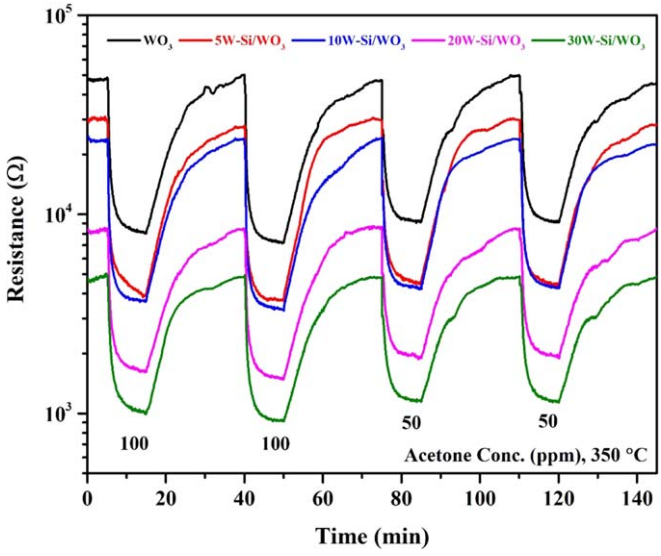

Figure 10. The dynamic acetone gas-sensing response of Si-doped WO_3 nanorods along with exposure to various acetone concentrations of 50 to 100 ppm at 350 °C.

good agreement with the low intensive Si distribution presented in the EDS map. The Si content tends to increase with increasing the input power of the Si source (figure 7(f)).

The surface chemical compositions and oxidation state of elements existing in 5 W Si/WO_3 film after testing were illustrated in figure 8. The survey scan spectrum (figure 8(a)) confirms that the expected material elements on the surface included W 4 f, O 1 s, and Si 2p as well as Carbon (C 1 s) due to surface contamination. Considering to W 4 f element (figure 8(b)), W $4f_{7/2}$ and W $4f_{5/2}$ core levels can be individually split into one doublet pair at binding energies of 35.60 and 37.72 eV, respectively. The binding energy difference of W 4 f doublet peaks is 2.12 eV, which could be assigned to the W^{6+} oxidation state [27]. For the oxygen (figure 8(c)), the curve of O 1 s peak can be decomposed into three peaks located at 530.50, 531.50, and 532.78 eV. The main O 1 s peak could be attributed to lattice oxygen (O^{2-}) while the middle and the last ones may be associated with chemisorbed surface oxygen (O^{-}) or weakly bonded oxygen species and hydroxide species since water molecules adsorbed on the surface, respectively [28]. Regarding the Si element (figure 8(d)), the Si 2p peak was found at the binding energy of 103.10 eV, indicating that the oxidation state of Si in the sample is Si° or metallic Si [29]. Therefore, there was the presence of metallic Si distributing on the WO_3 surface.

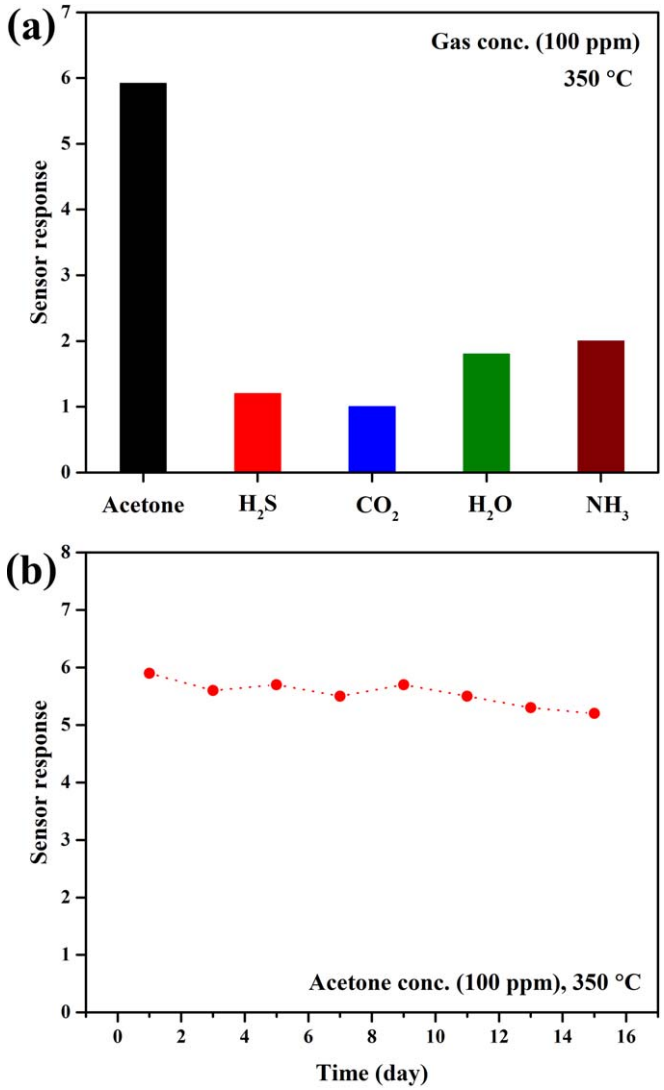

Figure 11. (a) Selectivity characterization of 5 W Si/WO_3 sensor exposed to various gases and (b) long-term stability of 5 W Si/WO_3 sensor towards 100 ppm acetone at 350 °C.

3.2. Gas-sensing properties

The gas sensing properties were characterized using a flow-through gas sensing system (figure 4). The operating temperature was an important factor influencing the surface states of the metal oxide and the chemical reaction. The response of the sensors based on Si-doped WO_3 nanorods towards 100 ppm acetone vapor tested at a different operating temperature ranging from 250 °C to 400 °C is presented in figure 9. It was obviously shown that the acetone response of each sensor initially increased to the highest response at an optimal temperature before decreasing when temperature increases. The optimum operating temperature for acetone gas-sensing examinations of various Si-doped WO_3 was around 350 °C. In addition, the acetone response was sustained significantly as the small amount of Si doping but then became decreasing as the Si doping content increased at all working temperatures. Especially, Si-doped WO_3 sensor displays the highest response of approximately 5.92 was deposited from input power 5 watts to silicon target and co-sputtering.

Figure 10 demonstrated changes in resistance of WO_3 sensors with different Si doping concentrations exposed to various acetone concentrations (50–100 ppm) at the optimum working temperature. The baseline resistance of the Si-doped WO_3 sensor seems to decrease with increasing Si doping contents. Reduction of WO_3 resistance by doping Si attributes the electrons transfer at the heterojunction. The electrons are transferred from Si particles to the WO_3 nanorods, then electrons accumulate at the surface of WO_3, leading to a reduction of the baseline resistance [30]. After being subjected to acetone vapor, the resistance of all sensors decreased, especially a resistance change of Si-doped WO_3 sensor significantly enhanced with Si doping at 5 W power of Si source before declining at the higher Si doping. It was an acetone detection at low concentration, the noise was observed during acetone exposure due to the fluctuation of acetone concentration from the bubbling process. It could be seen that the increasing response of acetone for all sensors when increasing acetone concentration. The result

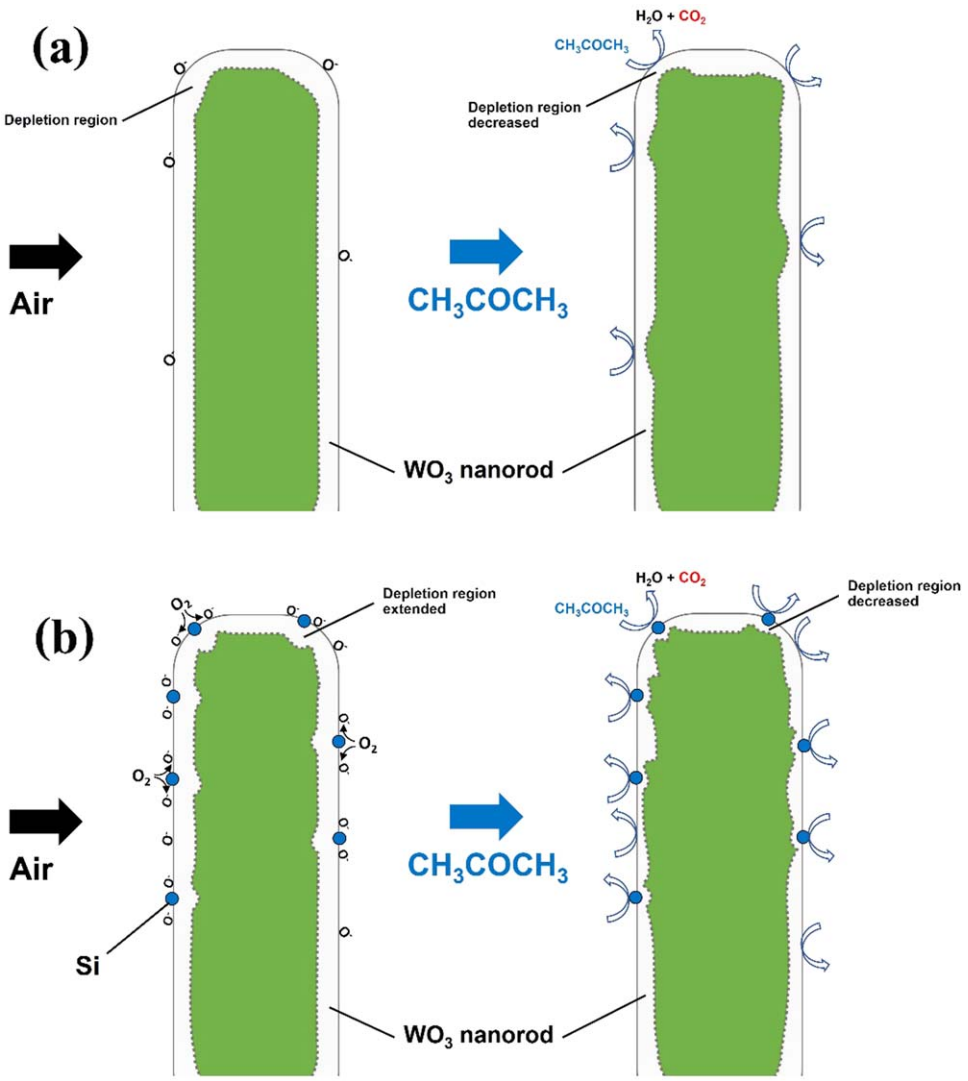

Figure 12. Schematic diagram of the possible gas-sensing mechanism of (a) pure WO_3 and (b) Si-doped WO_3 nanorod on exposure to acetone vapor.

implied that an increased number of acetone molecules interacted with adsorbed oxygen species on the surface of WO_3. Moreover, the sensor response improves substantially at the Si doping content at the 5 W power source, which offers the highest acetone response of approximately 5.92 at 100 ppm. Regarding the response dependency on acetone concentration, the optimal sensor shows a low detection limit at 50 ppm with a response of around 5.20. Lastly, the acetone selectivity of the optical sensor (5 W Si/WO_3) was investigated against 100 ppm H_2S, CO_2, H_2O, and NH_3 at the working temperature of 350 °C, as illustrated in figure 11(a). It is seen that the sensor exhibited a higher acetone response than other gases, revealing that the sensor presents excellent acetone selectivity. Figure 11(b) demonstrates the sensor response of the 5 W Si/WO_3 sensor towards 100 ppm acetone at 350 °C for 15 days. It shows that the acetone response of the 5 W Si/WO_3 sensor is relatively stable with a fluctuation of ~20%. Therefore, Si-doped WO_3 sensor can be an attractive choice for acetone detection that has a great potential for breath analysis.

The acetone gas sensitivity was investigated from the prepared Si-doped WO_3 nanorods at different electrical input power applied to the Si sputtered target. Mechanism of the gas sensor based on the analysis of the characteristics of above gas sensing. The sensing mechanism of the Si-doped WO_3 nanorod-based sensor could be created by using the surface-controlled model. WO_3 nanorods were normally n-type semiconductors, in which electrons became the major charge carriers and played an essential role in electrical properties. Then, oxygen molecules could be easily formed chemisorbed oxygen species (O^- or O^{2-}) [21, 31, 32] by trapping one or two electrons at the surface of WO_3 nanorods, which caused an increase of electron depletion region of the surface of WO_3 nanorods and increasing its resistance.

Under the acetone gas exposure (figure 12(a)), the acetone molecules reacted with chemisorbed oxygen partners on the surface of WO_3 nanorods, releasing free-electron back to the WO_3 nanorods. Consequently, the

thickness of the depletion region decreases, leading to a reduction of resistance of WO_3 nanorods, which is in good agreement with the experimental result in figure 10. The reaction can be expressed by following equations (1)–(2) [13, 15, 33, 34].

$$CH_3COCH_3 + 8O^-_{(ads)} \rightarrow 3CO_{2(g)} + 3H_2O_{(g)} + 8e^- \quad (1)$$

$$CH_3COCH_3 + 8O^{2-}_{(ads)} \rightarrow 3CO_{2(g)} + 3H_2O_{(g)} + 16e^- \quad (2)$$

With Si doping on the WO_3 nanorods, Si particles can improve acetone sensing performance in two different ways. Firstly, Si particles can be acted as catalytic for the oxygen spill-over process in Si- WO_3 nanorods [34]. When the air exposure to the system, Si-doped WO_3 nanorods can dissociate O_2 into O^-, and then O^- overflow adsorbs onto the WO_3 surface (figure 12(b)). Then Si particles reduced the activation energy required for the reaction and further enhance its response to acetone. Secondly, doping with Si can induce a large surface area. The gas response is commonly proportional to the gas-surface area interaction [34]. More and more surface-active sites by optimal Si dopants led to improve the acetone response. Therefore, the presence of Si-doped WO_3 nanorods promotes additional surface-active sites and regeneration of electrons by enhancement of gas-chemisorbed oxygen interactions, leading to the overall improvement of the response.

The fast response-recovery time is greatly ascribed to more surface-active sites to promote interaction with acetone. The reactive magnetron co-sputtering with OAD technique provided the possibility for fabrication of well-ordered and sophisticated nanostructure, e.g. nanorods, nanocolumns by manipulating the deposition angle and substrate angle and fabrication Si-doped WO_3 nanorods prepared by magnetron sputtering as a sensitive layer for acetone detection.

4. Conclusion

The gas-sensing properties of Si-doped WO_3 nanorod films deposited by reactive magnetron co-sputtering with OAD and annealed at 400 °C for 4 h in the air were characterized in the presence of acetone at various concentrations. The results showed that 1.43% of Si-doped WO_3 nanorods exhibited the maximum response ($S = 5.92$) in the actual 100 ppm acetone at operating temperature 350 °C, purified dry air carrier. The process exposed in this work demonstrated the potential of high sensitivity acetone gas sensor at low concentration and can be used as a supplementary tool for diabetes monitoring.

Acknowledgments

The author would like to thank the Synchrotron Light Research Institute and Nation Electronic, Computer Technology Centre (NECTEC) and the Department of Physics and Materials Science, Faculty of Science, Chiang Mai University, for providing the experiment facilities and Centre of Excellence in biomechanics Medicine, the Suranaree University of Technology for financial support of this research. Special thanks to Dr Narong Chanlek, BL5.3: XPS, Synchrotron Light Research Institute (Public Organization) and to Mr Nutthaphat Thornyanadacha, Thai Microelectronics Center (TMEC).

Data availability statement

The data generated and/or analyzed during the current study are not publicly available for legal/ethical reasons but are available from the corresponding author on reasonable request.

ORCID iDs

Bura Sindhupakorn https://orcid.org/0000-0002-6070-7441

References

[1] Wang D 2019 Investigation of different materials as acetone sensors for application in type-1 Diabetes diagnosis. biomedical *Journal of Scientific & Technical Research.* **14** 14

[2] Wang Y *et al* 2021 Conductometric room temperature ammonia sensors based on titanium dioxide nanoparticles decorated thin black phosphorus nanosheets *Sensors Actuators B* **349** 130770

[3] Zhou Y, Wang Y, Wang Y and Li X 2020 Humidity-enabled ionic conductive trace carbon dioxide sensing of nitrogen-Doped $Ti_3C_2T_x$ MXene/polyethyleneimine composite films decorated with reduced graphene oxide nanosheets *Analytical Chemistry*. **92** 16033–42
[4] Turner C, Španěl P and Smith D 2006 A longitudinal study of methanol in the exhaled breath of 30 healthy volunteers using selected ion flow tube mass spectrometry *SIFT-MS Physiol Meas.* **27** 637
[5] Anderson J, Lamm W and Hlastala M 2006 Measuring airway exchange of endogenous acetone using a single-exhalation breathing maneuver *Journal of applied physiology*. **100 3** 880–9
[6] Saasa V, Malwela T, Beukes M, Mokgotho M, Liu C-P and Mwakikunga B 2018 Sensing technologies for detection of acetone in human breath for diabetes diagnosis and monitoring *Diagnostics (Basel)*. **8** 12
[7] Sun Y-F *et al* 2012 Metal oxide nanostructures and their gas sensing properties: a review *Sensors (Basel)*. **12** 2610–31
[8] Andrysiewicz W, Krzeminski J, Skarżynski K, Marszalek K, Sloma M and Rydosz A 2020 Flexible gas sensor printed on a polymer substrate for sub-ppm acetone detection *Electronic Materials Letters*. **16** 146–55
[9] Tomer V K, Singh K, Kaur H, Shorie M and Sabherwal P 2017 Rapid acetone detection using indium loaded WO_3/SnO_2 nanohybrid sensor *Sensors and Actuators B: Chemical*. **253** 703–13
[10] Yang W, Shen H, Ge J and Xu B 2021 Improving TiO_2 gas sensing selectivity to acetone and other gases via a molecular imprinting method *Nanotechnology*. **32** 155503
[11] Brudnik A, Czternastek H, Zakrzewska K and Jachimowski M 1991 Plasma-emission-controlled d.c. magnetron sputtering of TiO_{2-x} thin films *Thin Solid Films*. **199** 45–58
[12] Xu H *et al* 2019 Mesoporous WO_3 nanofibers with crystalline framework for high-performance acetone sensing *Frontiers in Chemistry*. **7** 266
[13] Chang X *et al* 2021 Highly sensitive acetone sensor based on WO_3 nanosheets derived from WS_2 nanoparticles with inorganic fullerene-like structures *Sensors and Actuators B: Chemical*. **343** 130135
[14] Muhammad Imran Ya E A, Wang T, Nunzio M, Tuquabo T, Prashant S and Mahnaz S 2020 Enhanced amperometric acetone sensing using electrospun non-stoichiometric WO_{3-x} nanofibers *Journal of Materials Chemistry C*
[15] Shi J *et al* 2011 WO_3 nanocrystals: synthesis and application in highly sensitive detection of acetone *Sensors and Actuators B Chemical*. **156** 820–4
[16] Righettoni M, Tricoli A and Pratsinis S E 2010 Si:WO_3 sensors for highly selective detection of acetone for easy diagnosis of diabetes by breath analysis *Analytical Chemistry*. **82** 3581–7
[17] Rydosz A, Szkudlarek A, Zj bka M, Domanski K, Maziarz W and Pisarkiewicz T 2016 Performance of Si-doped WO_3 thin films for acetone sensing prepared by glancing angle DC magnetron sputtering *IEEE Sensors Journal*. **16** 1004–12
[18] Zhang Y, He W, Zhao H and Li P 2013 Template-free to fabricate highly sensitive and selective acetone gas sensor based on WO_3 microspheres *Vacuum*. **95** 30–4
[19] Breedon M *et al* 2010 Synthesis of nanostructured tungsten oxide thin films: a simple, controllable, inexpensive, aqueous sol−gel method *Crystal Growth & Design*. **10** 430–9
[20] Liu S, Zhang F, Li H, Chen T and Wang Y 2012 Acetone detection properties of single crystalline tungsten oxide plates synthesized by hydrothermal method using cetyltrimethyl ammonium bromide supermolecular template *Sensors and Actuators B: Chemical*. **162** 259–68
[21] Chen D *et al* 2011 Effects of morphologies on acetone-sensing properties of tungsten trioxide nanocrystals *Sensors and Actuators B: Chemical*. **153** 373–81
[22] Xu X, Yazdi M A P, Sanchez J-B, Billard A, Berger F and Martin N 2019 Reactive co-sputtering of tungsten oxide thin films by glancing angle deposition for gas sensors *Materials Today: Proceedings*. **6** 314–8
[23] Bräuer G, Szyszka B, Vergöhl M and Bandorf R 2010 Magnetron sputtering—milestones of 30 years *Vacuum*. **84** 1354–9
[24] Charles C, Martin N, Devel M, Ollitrault J and Billard A 2013 Correlation between structural and optical properties of WO_3 thin films sputter deposited by glancing angle deposition *Thin Solid Films*. **534** 275–81
[25] Zhang J, Cao Y, Gao Q, Wu C, Yu F and Liang Y 2013 Template-assisted nanostructure fabrication by glancing angle deposition: a molecular dynamics study *Nanoscale Research Letters*. **8** 312
[26] Zhao Y, Ye D, Wang G C and Lu T-M 2003 Designing Nanostructures by glancing angle deposition. proceedings of spie - the international society for *Optical Engineering*. **5219** 59–73
[27] Liang Y-C and Chao Y 2019 Enhancement of acetone gas-sensing responses of tapered wo_3 nanorods through sputtering coating with a thin SnO_2 coverage layer *Nanomaterials (Basel)*. **9** 864
[28] Liang Y-C and Chang C-W 2019 Improvement of ethanol gas-sensing responses of ZnO¯WO_3 composite nanorods through annealing induced local phase transformation *Nanomaterials (Basel)*. **9** 669
[29] Demchenko I N, Melikhov Y, Syryanyy Y, Zaytseva I, Konstantynov P and Chernyshova M 2018 Effect of argon sputtering on XPS depth-profiling results of Si/Nb/Si *Journal of Electron Spectroscopy and Related Phenomena*. **224** 17–22
[30] Li S, Yao Z, Chow G, Zhang R and Shen H 2017 Fabrication and characterization of WO_3 thin films on silicon surface by thermal evaporation *Materials Letters*. **15** 195
[31] Ren Y *et al* 2020 Synthesis of orthogonally assembled 3D cross-stacked metal oxide semiconducting nanowires *Nature Materials*. **19** 203–11
[32] Zhu Y *et al* 2017 Mesoporous tungsten oxides with crystalline framework for highly sensitive and selective detection of foodborne pathogens *Journal of the American Chemical Society*. **139** 10365–73
[33] Punginsang M, Wisitsoraat A, Tuantranont A, Phanichphant S and Liewhiran C 2019 Ultrafine Bi_2WO_6 nanoparticles prepared by flame spray pyrolysis for selective acetone gas-sensing *Materials Science in Semiconductor Processing*. **90** 263–75
[34] Lu W *et al* 2018 Great enhancement of CH_4 sensitivity of SnO_2 based nanofibers by heterogeneous sensitization and catalytic effect *Sensors and Actuators B: Chemical*. **254** 393–401